Study of the violent collisions between ^{63}Cu+ ^{232}Th at 35 MeV/nucleon

J. Cibor, Z. Majka,* T. Kozik, P. Staszel, and Z. Sosin
Institute of Physics, Jagellonian University, ul. Reymonta 4, 30-059 Kraków, Poland

K. Hagel, J. Li, L. Lou,† R. Tezkratt,‡ D. Utley, R. Wada, B. Xiao, and J.B. Natowitz
Cyclotron Institute, Texas A&M University, College Station, Texas 77843
(Received 15 July 1996)

A study of the decay of hot and heavy composite nuclei produced in the violent collisions between ^{63}Cu and ^{232}Th at 35*A* MeV is presented. The measurement of fission fragment correlations indicates that ~ 70% of the projectile linear momentum can be transferred to the fissioning system. Heavy reaction products were observed at a laboratory angle of $\theta=6°$ in coincidence with neutrons, light charged particles, and intermediate mass fragments. The dynamical aspects of the collisions between the projectile and target nuclei were investigated using the computer code CHIMERA which is based upon the molecular dynamics concept. Asymptotic characteristics of the reaction products were confronted with results of calculations of the tandem CHIMERA plus GEMINI codes. The data and model comparisons show that a composite system of mass as high as 275 amu and with an excitation energy ~ 1 GeV is formed in the most violent collisions. Some of the heavy reaction remnants are located on the fragment mass versus velocity plane inside the area where the evaporation residues resulting from the decay of the hot composite system are expected. A high neutron multiplicity associated with these events indicates their origin in the most dissipative events. However, a low cross section for the production of these remnants and the close similarity of their characteristics to the fission fragments do not allow more conclusive statements. [S0556-2813(97)05801-9]

PACS number(s): 25.70.Jj, 02.70.Ns, 21.65.+f, 24.10.Lx

I. INTRODUCTION

Intermediate energy nucleus-nucleus collisions provide opportunities for studying properties of nuclear matter at densities and temperatures far different than those encountered in nuclei near their ground states. This provides an opportunity to probe the physics contained in the equation of state for infinite nuclear matter [1]. In particular, it was suggested by Bonche *et al.* [2] that a study of nuclei at the limit of the excitation energies which they can sustain can be used to verify parameters of the nuclear equation of state. Before any serious attempts can be made to approach this fundamental problem, two crucial questions concerning the formation and decay of hot nuclear systems produced in nuclear collisions have to be solved; i.e., what is the maximum excitation energy which can be deposited in a nucleus before complete disintegration, and what are the dominant mechanisms responsible for the decay of the excited nuclear system?

In order to pursue these problems an exclusive experiment that imposed strong restrictive conditions was performed at the Texas A&M K-500 superconducting cyclotron facility. A brief report of this work was published previously [3].

The paper is organized as follows. In Sec. II the experimental procedure is presented. Section III is devoted to a presentation of the experimental data. The dynamical aspects of the collisions and asymptotic characteristics of the reaction products are modeled in Sec. IV. A summary of the results and conclusions are given in Sec. V.

II. EXPERIMENTAL PROCEDURE

The 35*A* MeV ^{63}Cu beam was incident on the Thorium target which was ^{232}Th of 0.375 mg/cm^2 on 0.030 mg/cm^2 C backing. The detectors for the charged fragments were placed inside the scattering chamber of the 4π neutron ball detector [4] containing about 1800 liters of a gadolinium-loaded liquid scintillator. The scattering chamber has a cylindrical shape (45 cm high and 40 cm in diameter) with a wedge-shaped forward extension covering $\pm$ 20° in the horizontal plane. A multidetector arrangement constructed at the Institute of Physics of the Jagiellonian University was used mainly for detection of the light charged particles (LCP's) with $Z\leqslant 2$ and of intermediate mass fragments (IMF's) with $3\leqslant Z\leqslant 12$. The 35 ionization chamber, Si telescopes, which are modified versions of the telescopes described in Ref. [5], were located between 50° and 150° in the laboratory and each one covered 42 msr of solid angle. A thin window (0.1 mg/cm^2) and low operation pressure (isobutane at 135 torr) of the ionization chambers of the telescopes allowed low detection thresholds ($<0.5A$ MeV) for the LCP's and IMF's. The *E* detectors were 2 mm thick and 31 mm diam Si(Li) detectors. Four of these telescopes were tuned to detect fission fragments (FF's). The heavy residue Si detector was placed at 6° in a long extension tube 175 cm from the target. This detector was 900 mm^2 in area and 200 μm thick. Three Si detectors of large area and 300 μm thick were used for

*On sabbatical leave at Cyclotron Institute, Texas A&M University, College Station, Texas 77843.

†Present address: Human Genome Project, Lawrence Berkeley National Laboratory, 1 Cyclotron Road, Berkeley, California 94720.

‡Present address: 28 Chemin de la Bourdette, 31400 Toulouse, France.

fission fragment detection. Two of them labeled FF1 and FF2 were placed above and below the horizontal plane and covered the azimuthal angles from 34° to 70° and from 36° to 72° in the laboratory, respectively. These detectors were 6 cm long and 4 cm wide and divided into seven strips set horizontally. A third detector (FF3) was 5×5 cm^2 and placed in the horizontal plane on the left side of the beam and covered the range from 9.5° to 14.5°. The projectilelike fragment hodoscope was located on the other side of the beam. The hodoscope, consisting of one 5×5 cm^2 area and 150 μm thick Si detector, backed with a CsI crystal 6×4 cm^2 area and 0.5 cm thick, covered a range from 5° to 7°. Two Si detectors sited at $\pm$ 2° were used as monitors.

The efficiency calibration of the neutron ball was done by using a ^{252}Cf source and a computer simulation employing the computer code DENIS [6–8]. This simulation takes into account the source dynamics of the emitters. The energy calibrations of all the charged particle detectors were performed by using α particles from the ^{148}Gd and ^{252}Cf sources and the two-yield maxima in the ^{252}Cf fission fragment energy spectrum. The total pulse height defects for the fission fragments were obtained by putting the fission fragment detector inside the chamber and adjusting of the gas pressure in the chamber. The total pulse height defect for the residue detector was determined using ^{252}Cf and scattered and degraded beams of 2A MeV ^{181}Ta and ^{136}Xe. Timing calibrations were made using delay lines in the timing circuits. Plasma delays were determined according to the measured times and known timing of the scattered reference beam.

III. EXPERIMENTAL RESULTS

A. Fission fragments

During the past decade, there has been much discussion about a saturation in the energy deposition in the collisions of heavy and asymmetric nuclei. The decline in the cross section for the fusion-fission process investigated in terms of the folding angle distributions has been interpreted as indicating that, at beam energies above 30A MeV, the energy deposition saturates [9]. However, this is inconsistent with studies of the ^{40}Ar + ^{232}Th reaction reported in Ref. [8] and of a very recent study of the FF's, IMF's and LCP's produced in ^{40}Ar + ^{232}Th collisions at $E_{\rm beam}$ = (15–115)A MeV, which indicates no saturation in the deposited energy in the central collisions of this system in the bombarding energy range studied [10].

In the present analysis, we use a variety of measures to establish the energy deposition in the violent collisions of ^{63}Cu + ^{232}Th at 35A MeV. Since linear momentum transfer (LMT) and excitation energy are very closely related quantities, the fission fragment correlations have been investigated. The reconstructed characteristics of the fusion-fission process were obtained from the measured energies and the angles of two detected fission fragments. Since we have no knowledge of their masses and velocities, we apply a kinematical reconstruction procedure to achieve a description of the fission events. A few assumptions have to be made. The first assumption is that the angular distributions of particles emitted from the compound nucleus and from the fission fragments are isotropic in the source frames, and so the mean velocities of the recoiling compound nucleus and the fission fragments are not affected on the average. We assume also that the reaction is a binary one (we will address this issue in following sections).

Applying the momentum conservation principle at the scission point we can evaluate the fission fragment masses:

$$M_1^{\rm sc}=\frac{M_{\rm tot}E_2^{\rm sc}\sin^2\theta_2}{E_1^{\rm sc}\sin^2\theta_1+E_2^{\rm sc}\sin^2\theta_2} \tag{1}$$

and

$$M_2^{\rm sc}=\frac{M_{\rm tot}E_1^{\rm sc}\sin^2\theta_1}{E_1^{\rm sc}\sin^2\theta_1+E_2^{\rm sc}\sin^2\theta_2}, \tag{2}$$

where $E_1^{\rm sc}$ and $E_2^{\rm sc}$ are the fission fragment energies, θ_1 and θ_2 are the angles of emitted fission fragments, and $M_{\rm tot}$ is a total mass of a fissioning system. All those values are for the scission point.

$M_{\rm tot}$ is actually not known. We estimate this mass in the following way. For a given LMT the massive transfer hypothesis is applied to predict the mass ($M'_{\rm tot}$) and excitation energy of the compound nucleus after the preequilibrium emission. The previous works (see, e.g., [11] and [12]) show that fission is a relatively slow process and it takes place at low excitation energy ($\sim$ 150 MeV). We also assume that the prescission light particle emission takes 15 MeV per nucleon on the average. From the excitation energy calculated for a given LMT we have subtracted 150 MeV and divided the remainder by 15 MeV. Thus we have obtained an approximation to the number of particles evaporated before scission ($M_{\rm CN}^{\rm ev}$). In order to get $M_{\rm tot}$ we have subtracted that value from $M'_{\rm tot}$ For the LMT which could be investigated by our set up of the FF detectors, the resulting mass $M_{\rm tot}$ was about 225 and that value has been used in the data analysis.

The velocity of the compound nucleus at the scission point is given by

$$V_{\rm CN}=\sqrt{\frac{2E_1^{\rm sc}E_2^{\rm sc}}{M_{\rm tot}(E_1^{\rm sc}\sin^2\theta_1+E_2^{\rm sc}\sin^2\theta_2)}}\sin(\theta_1+\theta_2). \tag{3}$$

All of the above equations are valid at the scission point only. To apply them to the measured quantities we have to take into account postscission emission. Under the assumption that the light particle emission is isotropic in the source frame, the velocities and the trajectories of fission fragments are not changed on the average. However, the masses and the energies of the fission fragments are changed.

In the case of symmetric fission, when each fission fragment emits $m_{\rm frag}^{\rm evap}\approx5$ particles we have the following relation between the fragment energies at the scission point and those measured by the detectors:

$$E_{1,2}^{\rm sc}=E_{1,2}\times\frac{M_{1,2}^{\rm sc}}{(M_{1,2}^{\rm sc}-m_{\rm frag}^{\rm evap})}. \tag{4}$$

Thus, the compound nucleus velocity [Eq. (3)] can be expressed by the measured quantities (fission fragment kinetic energies and emission angles):

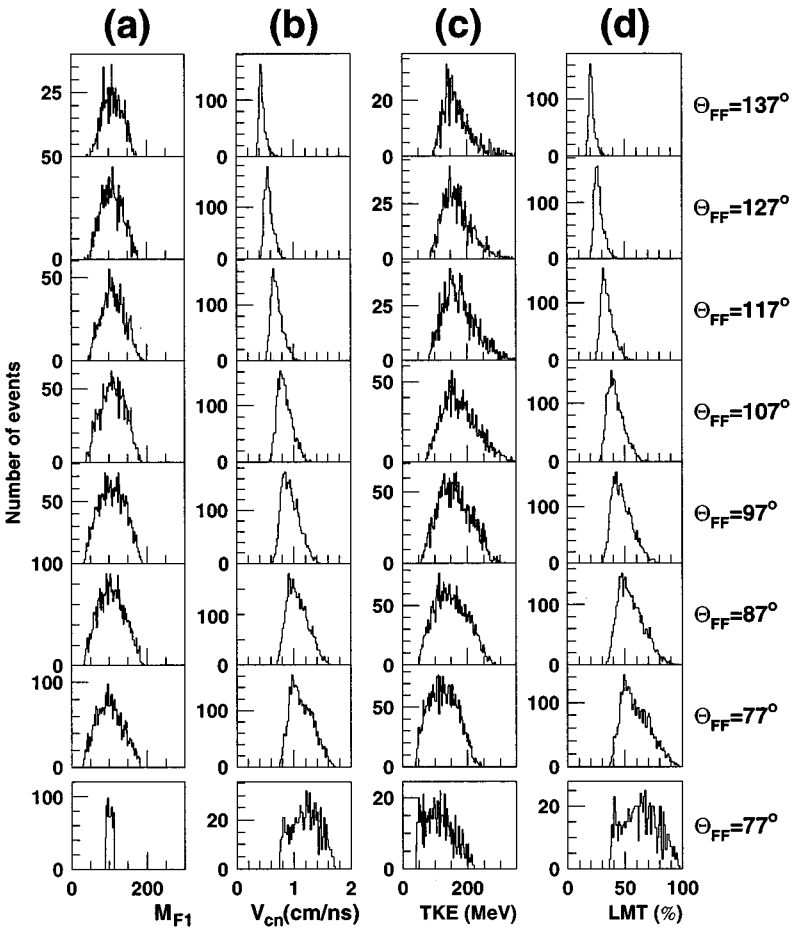

FIG. 1. Reconstructed characteristics of the fission process (see text).

$$V_{\mathrm{CN}}=\sqrt{\frac{2E_1E_2}{(M_{\mathrm{tot}}-2m_{\mathrm{frag}}^{\mathrm{evap}})(E_1\sin^2\theta_1+E_2\sin^2\theta_2)}}\sin(\theta_1+\theta_2). \tag{5}$$

Now, assuming that the unfused part of the projectile escapes forward with the beam velocity, the LMT, ρ, to the fused system is given as

$$\rho=\frac{M_{\mathrm{target}}}{M_{\mathrm{projectile}}}\frac{V_{\mathrm{CN}}}{(V_{\mathrm{projectile}}-V_{\mathrm{CN}})}. \tag{6}$$

Figure 1 displays the resultant mass distributions [column (a)] and the energy spectra [column (c)], when one of the fission fragments is detected by the FF1 detector in coincidence with the second fission fragment, detected by the FF2 detector. The velocities of the fissioning system and the LMT are shown in columns (b) and (d), respectively. Symmetric detection angles for both fission fragments were selected. The bottom row in Fig. 1 shows the results obtained imposing the condition of symmetric fission with both masses of the fragments detected at $\theta_{\mathrm{FF}}=77°$ equal to the most probable value of the observed fission fragment mass distribution, ± 10 amu. Here, one can notice that the most probable value of the LMT is located in the vicinity of 70%. Assuming a simple massive transfer hypothesis, the LMT can be used to estimate the excitation energy of the fused system. Figure 2 shows the derived excitation energy of the fused system obtained by assuming that the unfused projectile fraction escapes with the beam velocity. The circles and squares represent, respectively, the results obtained assuming that the unfused projectile fraction escapes as one piece of nuclear matter or as a collection of separated

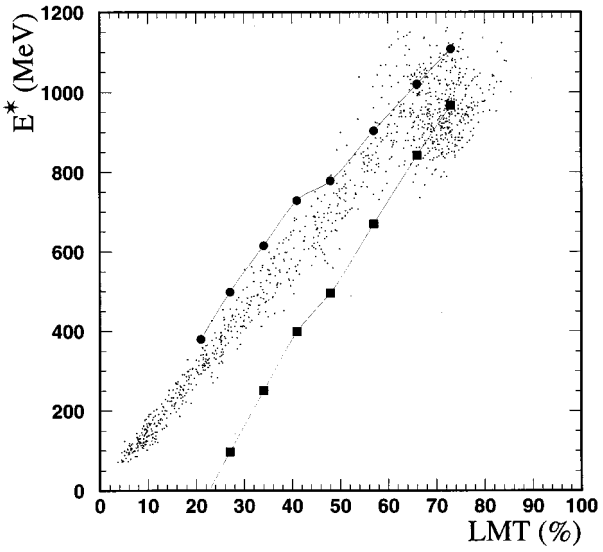

FIG. 2. The calculated excitation energy of the fused system versus the linear momentum transfer. The solid circles and squares represent the results which have been obtained assuming that the unfused projectile fraction escapes with the beam velocity as one piece of nuclear matter and as a collection of separated nucleons, respectively. The small dots represent the CHIMERA code results for the central collisions.

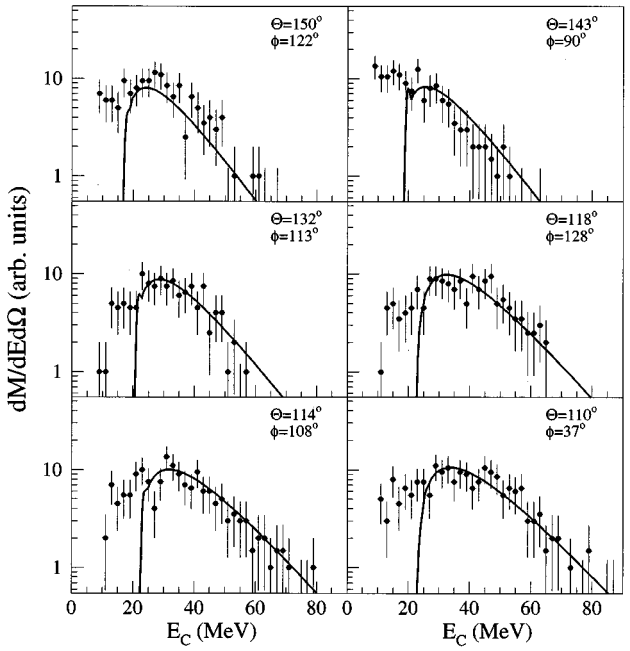

FIG. 3. The inclusive energy spectra of carbon fragments (dots). Solid lines were obtained from a global fit with a single compound nucleus source.

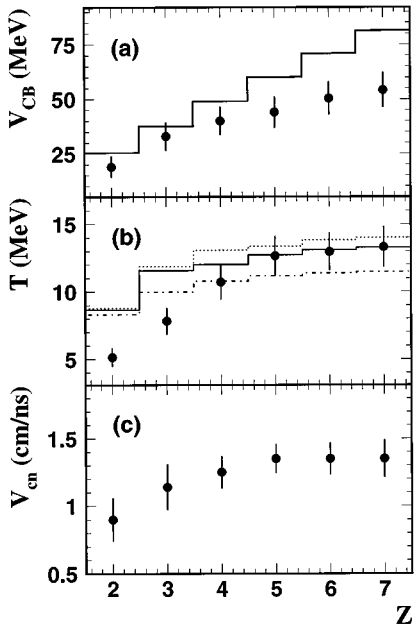

FIG. 4. Characteristics of the compound emission source obtained from a global fit (dots). The solid dots represent experimental data. The histogram in the upper panel shows the calculated Coulomb barriers for a spherical shape of the daughter nucleus obtained from systematics [15]. Histograms in the middle panel show results of model calculations (see text).

nucleons. This indicates that, at the highest observed experimental value of the LMT, the fused system can acquire above 1 GeV excitation energy. Although this intuitive relation between the LMT and the excitation energy is useful, the precise link of both quantities has been modeled (see area indicated by the dots in Fig. 2) and results are discussed in the next section.

B. Light charged particles and intermediate mass fragments

The emission of the IMF's is an important decay mode of highly excited nuclear systems formed in proton-nucleus and nucleus-nucleus collisions. A variety of mechanisms that could be responsible for fragment production have been suggested [13]. Conventional statistical models have very successfully reproduced many features of the fragment data. In order to recognize the collision product deexcitation pattern, the experimental energy spectra of the LCP's and IMF's have been analyzed in terms of a multisource fit method. The fitted energy distributions of evaporated charged fragments in the source rest frame have been parametrized in the form [14]

$$\frac{d^2\sigma}{d\Omega\, dE} \sim \frac{M}{4\pi T^2}(E - V_{\mathrm{CB}}) \times \exp[-(E - V_{\mathrm{CB}})/T], \quad (7)$$

where M is the particle multiplicity, T is the temperature parameter, and V_{CB} is the Coulomb energy of the particle. Since the LCP and IMF telescopes were located predominantly at the backward hemisphere, we expect that the energy spectra recorded by these detectors originate mainly from the deexcitation of the heavy and hot composite system formed in the massive transfer process. In Fig. 3 we show the inclusive energy spectra of the carbon fragments (solid points). The global fits to the backward angle spectra with one moving source are shown as the solid lines. In this analysis the particle multiplicity, the quantities T and V_{CB} and the moving source velocity V_{CN} were treated as adjustable parameters in the least–squares fitting procedure. Fits like those shown in Fig. 3 were made for fragments with $2 \leqslant Z \leqslant 7$ and the fitted parameters that characterize the moving source are plotted in Fig. 4 and listed in Table I. For increasing Z of the IMF, the values of V_{CB} were found to be systematically lower than those calculated (histogram) from systematics [15] which assumes a spherical shape of the daughter nucleus. This observation suggests that the heavier IMF's are emitted from a more deformed system. However, our measurements do not allow us to exclude other factors, such as cooling, expansion, and secondary decays, which can affect the height of the Coulomb barriers. Both the temperature parameter and the source velocity show a correlated dependence on the Z value of the IMF (a lower source velocity indicates that a lower value of the linear momentum was transferred to the composite system producing a less excited source). However, the LMT range which corresponds to the deduced source velocities cannot account for a large temperature variation between the light and heavy IMF's. Another effect which might cause the observed trend in the temperature parameter dependence on the Z value of the IMF can be explored in terms of a model based on random walk in momentum space [16]. In this model, the fragment momentum is obtained by summing up the momentum vectors of its constituent nucleons. The solid line histogram in Fig. 4(b) was obtained [17] assuming that a decaying ensemble of nucleons has temperature (internal) $T_{\mathrm{in}} = 6$ MeV and a freeze-out density of $0.85\rho_0$. This value of the freeze-out density was obtained with the CHIMERA simulations (see Sec.

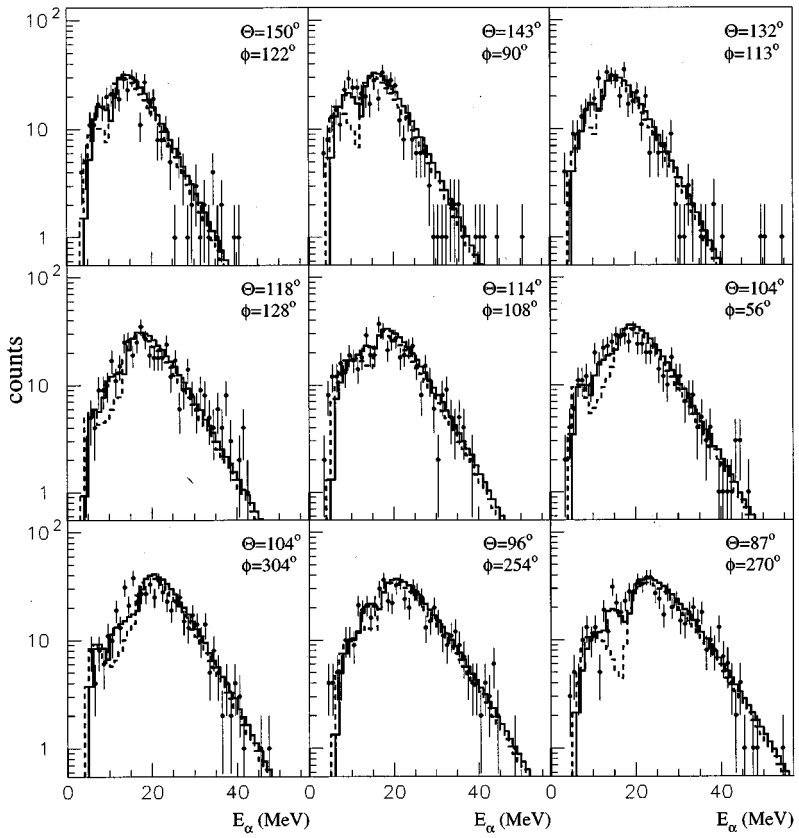

FIG. 5. The inclusive α particle energy spectra (dots). Dashed lines represent a global fit obtained with three sources (a compound nucleus and two fission fragments). Solid lines were obtained when these three moving sources were supplemented by an additional near scission emission source.

IV and Ref. [18]). Here, the experimental spectral slopes are well reproduced by the model calculations for $Z>3$. A variation of the model spectral slope temperatures with the internal temperature and density of the decaying system is shown by dashed ($T_{\rm in}$ = 5 MeV and $\rho=\rho_0$) and dotted ($T_{\rm in}$ = 6 MeV and $\rho=\rho_0$) line histograms in Fig. 4(b).

Although the higher energy parts of the fragment kinetic energy spectra are rather well described by assuming one moving source, there are significant discrepancies in low energy fits. Taking into account that α particle spectra have much better statistics than the IMF spectra, the α spectra measured in coincidence with two near symmetric fission fragments $[0.3<M1/(M1+M2)<0.7]$ were carefully examined. The FF's were detected at the symmetric angles. Central collisions with the LMT larger than 50% were selected by a condition that sets an appropriate gate on the FF folding angle. In this case, global fits with three moving sources have been used to reproduce the experimental α particle spectra. The dashed curves shown in Fig. 5 represent the results of fits in which emission from the composite system and from the fully accelerated FF's was assumed. As is seen from Fig. 5, the combined yield from the three assumed sources of α particles reproduces quite well the observed distributions. However, in a few detectors (e.g., at $\theta=143°$, ϕ = 90° and θ = 87°, ϕ = 270°) a considerable excess of the observed yields above the global fit predictions is present.

The near-scission emission (NSE) of α particles has been reported by several groups [19]. In a succeeding analysis, we introduced an additional source of α particles that moves with the velocity of the composite system but that emits, on the average, α particles of lower energies. The solid curves shown in Fig. 5 represent results of fits in which this α particle emission from the neck region has been included in addition to the emission from the composite system and the fully accelerated FF's. The yield of this additional component was determined individually for each detector by requiring the best fit of the combined yield of all assumed sources. In Fig. 6 we show the angular dependence of the NSE yield. The angle Ψ is that between the velocity vector of the α particle direction and the fission axis, measured in the rest frame of the fissioning nucleus. The result presented in Fig. 6 demonstrates that the α particles originating from the neck source are emitted preferentially in the direction perpendicular to the fission axis. In Table II, the fitted parameters are listed. The multiplicity of α particles emitted from the neck source was derived from the data in Fig. 6.

We mentioned before that one-moving-source fits to the IMF spectra do not reproduce correctly the low energy region. However, our calculations indicate that this low energy fragment can originate from the neck region emission as well from the secondary decay of the excited heavier species. The inclusive data are not a sufficient constraint to disentangle the origin of these low energy fragments.

C. Neutron multiplicities

The conventional folding-angle technique, which has been used in Sec. III A as a tool to determine the LMT from the laboratory angle of the correlated FF's, has several uncertainties at the projectile mass and energy investigated in the present experiment. At 35*A* MeV beam energy, even for a violent collision, a largely varying fraction of the projectile can be captured by a target nucleus and the LMT is not

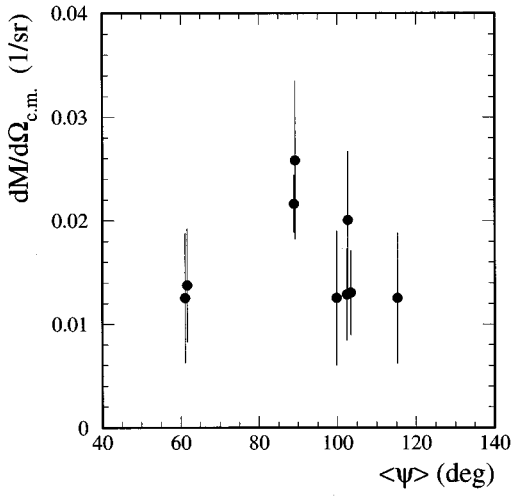

FIG. 6. The angular dependence of the near-scission emission source yield for the α particles.

precisely determined because the transferred mass is not accessible experimentally. Furthermore, an escaping mass causes a non-negligible transverse momentum component which together with a recoil of the fused system induced by the IMF emission leads to a broad momentum distribution (see Fig. 1).

In order to have a better insight into the reaction scenario when the highest amount of the available energy is deposited in the composite system, we have detected neutrons in coincidence with the charged reaction products. For the neutron-rich nuclei produced in the ^{63}Cu + ^{232}Th reaction, neutron evaporation is a dominant emission process and above 50% of the thermal energy is carried away by neutrons.

The experimental neutron distributions presented in this paper include background corrections but no efficiency corrections. The inclusive neutron multiplicity spectrum [Fig. 7(a)] exhibits two components that can be attributed to peripheral (at lower multiplicity) and central (at higher multiplicity) collisions [20]. As already observed in Fig. 1, the FF detectors cover the folding-angle range which selects large momentum transfers to the fissioning system. In Figs. 7(b)–7(e), we show the neutron multiplicity spectra when two near-symmetric FF's have been used to trigger the neutron measurement. The FF's have been detected at the near-symmetric angles and the corresponding folding-angle ranges are indicated in each panel. Here we observe that the shift of the neutron distribution to a lower multiplicity with an increasing folding angle (decreasing LMT) is small. Despite the fact that our detection system selects events with an apparent LMT range from 20% to 75% (see Fig. 1), the centroid of the neutron distribution shifts by only three neutrons (by four after efficiency correction). This result appears to reflect both fluctuations in the folding angle induced by particle emission and increasing competition of charged particle emission as the excitation energy increases. It should be noted that, at 20% LMT, the compound nucleus can be excited above 400 MeV.

We have already shown in Sec. III B that the IMF's are predominantly emitted from the hot composite system before scission. In Fig. 7(f) we show the neutron multiplicity spectrum when neutron counting was triggered by the detection of an IMF in the backward hemisphere. As expected, the IMF emission is associated with high neutron multiplicities. The results of the model calculations which are shown in Fig. 7 by the dashed and dotted lines will be discussed in the next section.

TABLE I. The global fit parameters for the inclusive IMF spectra.

Z	M	$T_{\rm app}$ (MeV)	$V_{\rm CB}$ (MeV)	$V_{\rm CN}$ (cm/ns)
3	0.097 ±0.009	7.8 ±1.00	33.0 ±4.9	1.14 ±0.14
4	0.041 ±0.005	10.7 ±1.19	40.0 ±5.8	1.25 ±0.14
5	0.035 ±0.006	12.5 ±1.35	46.2 ±6.7	1.31 ±0.12
6	0.037 ±0.007	12.9 ±1.31	50.4 ±6.6	1.35 ±0.11
7	0.025 ±0.007	13.3 ±1.55	54.3 ±7.2	1.35 ±0.12

To provide an overall view of the cooling pattern of the hot composite system by different deexcitation channels, we define the normalized differential multiplicity by the following relation:

$$\frac{d^2\sigma}{d\Omega dM_n} = \left(\frac{4\pi N_{\rm CF}}{\Omega N_{n,\rm incl}}\right)_{M_n}, \tag{8}$$

where $N_{\rm CF}$ is the number of charged fragments (CF's) observed in the backward hemisphere with a solid angle Ω and associated with the neutron multiplicity M_n. $N_{n,\rm incl}$ is the number of events with the neutron multiplicity M_n observed with the neutron ball running in the inclusive mode.

Several noteworthy features of the cooling pattern can be obtained from Fig. 8. First of all, neutron multiplicity thresholds are observed for the all CF emission. In other words, the CF emission is allowed if a sufficient amount of excitation energy has been transferred to the system. Once the threshold has been passed, the CF multiplicities increase roughly linearly with the measured neutron multiplicity, until the detected neutron multiplicity reaches a value $\langle M_n\rangle \approx 42$ which is somewhat larger than the location of the maximum of the neutron multiplicity distribution obtained for the largest LMT [see Fig. 7(e)]. In the high multiplicity tail of the neutron multiplicity distribution, the emission of the charged particles and IMF's stays constant within the statistical uncertainties. This feature may be interpreted as a statistical balance between the neutron and charged particle evaporation.

To recognize further the deexcitation pattern of the hot compound nucleus, the backward angle α particle spectra were sorted according to six neutron multiplicity bins: (0,18), (19,25), (26,32), (33,40), (41,50), and (51,60). The results of the global fit are given in Table III. Here, one can

TABLE II. The global fit parameters for the α particle spectra detected in coincidence with two fission fragments.

$Z=2$	M	$T_{\rm app}$ (MeV)	$V_{\rm CB}$ (MeV)	$V_{\rm CN}$ (cm/ns)
CN	1.37 ±0.11	5.18 ±0.25	18.40 ±1.4	0.87 ±0.07
NSE	0.08 ±0.03	3.50 ±0.31	13.78 ±1.1	0.87 ±0.07
per FF	0.3 ±0.02	3.24 ±0.29	11.90 ±1.0	1.56 ±0.12

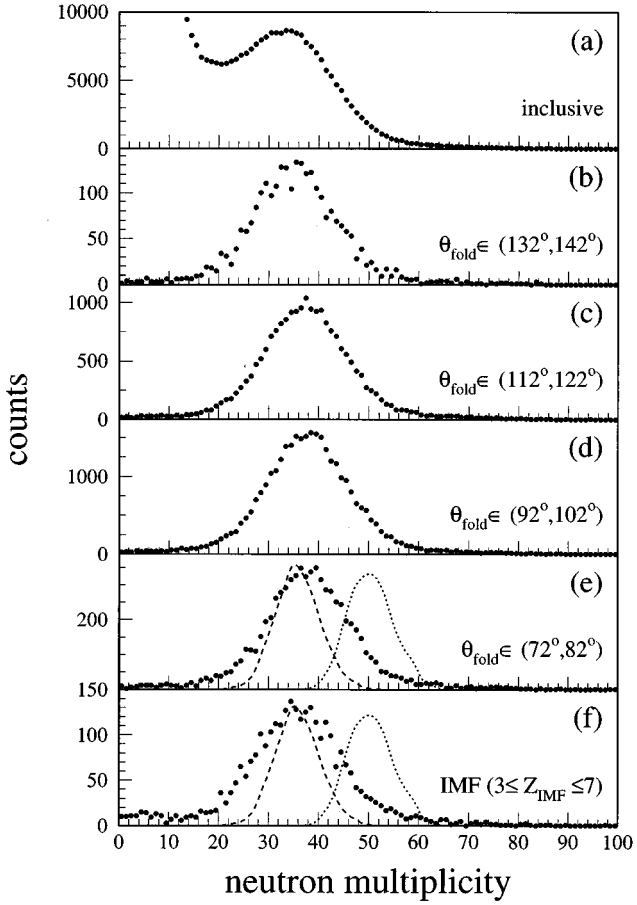

FIG. 7. The experimental neutron multiplicity spectra (dots) after background correction and without efficiency corrections. Panel (a) shows the inclusive neutron multiplicity spectrum, and panels (b)–(e) show the neutron multiplicity spectra when two near symmetric FF's have been used to trigger the neutron measurement. In panel (f) we show the neutron multiplicity spectrum when neutron counting was triggered by the detection of an IMF in the backward hemisphere. The results of the model calculations are shown by the dashed and dotted lines (see text).

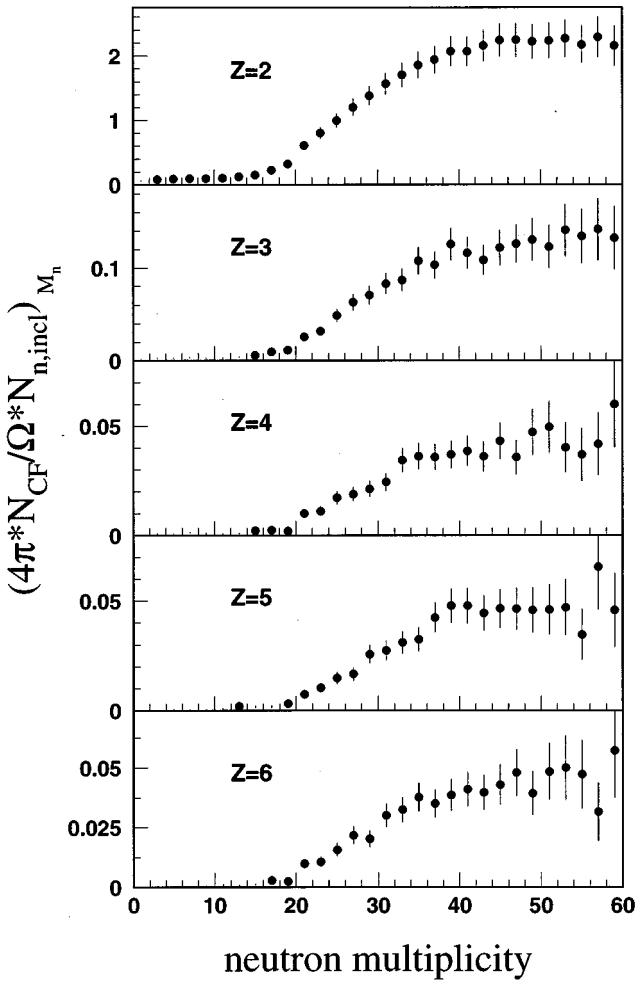

FIG. 8. Differential multiplicity for the α particles and IMF's as a function of the detected neutron multiplicity.

see also that the α particle [multiplicity levels off at the highest neutron multiplicity bin, however, the alpha particles are more energetic (spectral temperature is the highest for the highest neutron multiplicity bin). This observation, that the highest neutron multiplicity selects the hottest nuclei is in agreement with the highest velocity of the system.

Using the same neutron multiplicity gate bins, we investigated the charge distribution of the IMF's emitted into the backward hemisphere. These experimental charge distributions for $3 \leqslant Z \leqslant 9$ were fitted by a power law. The charge distributions are much flatter for higher neutron multiplicity bins and the apparent exponent τ stays constant at the value of 1.50 ± 0.05 for the neutron multiplicities higher than 25.

Combining together all observations presented above indicates the following scenario for deexcitation of the hot and heavy nuclei. At excitation energy below 300 ± 50 MeV the heavy system deexcites predominately by neutron emission (see also Fig. 3 in Ref. [8] where model calculations are presented). At higher excitation energies, the emission of the charged particles and fragments contributes strongly to the cooling process and the neutron multiplicity changes slowly with increasing excitation energy.

D. Heavy residues

We have shown in the former sections that, in the violent collisions between the ^{63}Cu and ^{232}Th at 35A MeV, the statistical deexcitation by the neutrons, LCP's, and IMF's follows the formation of the hot composite system and the fission occurs at the end of the evaporation chain. Such a delay of the fission process might favor the survival of heavy residues. Observations of heavy residues have been reported re-

TABLE III. The global fit parameters for the α particle spectra gated on the neutron multiplicity.

M_n gate	M	T_{app}(MeV)	V_{CB} (MeV)	V_{CN} (cm/ns)
0–18	0.11 ± 0.02	-	-	-
18–25	0.23 ± 0.03	4.23 ± 0.19	18.8	0.48 ± 0.14
25–32	1.40 ± 0.15	4.75 ± 0.25	19.0	0.90 ± 0.11
32–40	1.86 ± 0.21	5.05 ± 0.23	19.5	1.04 ± 0.15
40–50	2.17 ± 0.25	5.12 ± 0.23	19.7	1.05 ± 0.11
50–60	2.17 ± 0.27	5.41 ± 0.45	19.4	1.05 ± 0.16

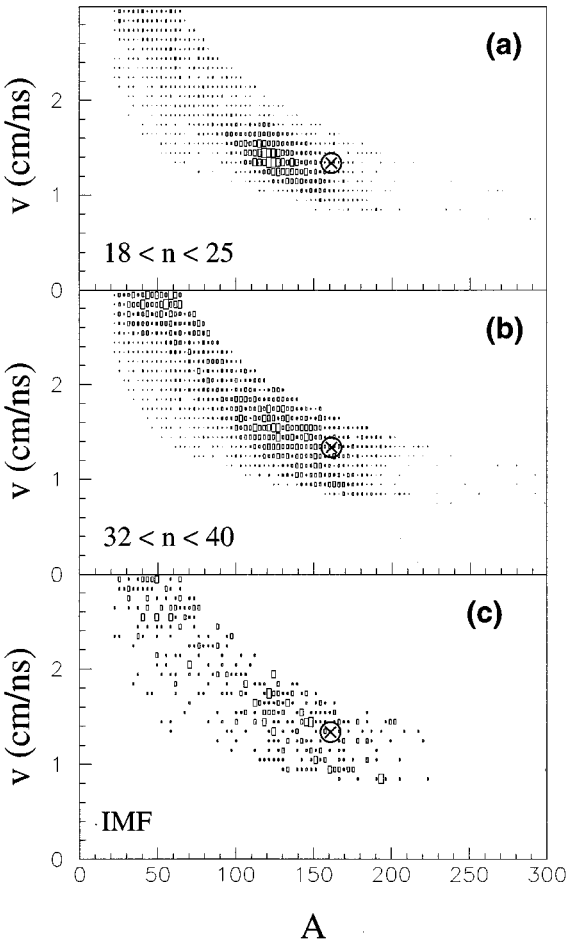

FIG. 9. The scatter plot of the number of events versus the mass and velocity for the heavy fragments detected by the hodoscope. The circles show the area where heavy residues are predicted by the CHIMERA-GEMINI model calculations.

cently in radiochemical measurements [21] as well as by using direct detection techniques [8,22].

Focusing on the reaction products at small forward angles we present in Fig. 9 scatter plots of the number of events versus the mass and velocity of heavy fragments detected by the hodoscope. Panels (a) and (b) show the results obtained by introducing the neutron multiplicity gate requirement indicated in each panel by the numbers in the brackets. One can see that the fission fragment events form a well-separated island of events and the heavy survivors of the composite system deexcitation are populated with much lower statistics. An expected area where the heavy surviving residues should be located is marked by the crossed circles (see discussion in the following section). Additional coincidence conditions [e.g., that at least one IMF was detected in the backward hemisphere as shown in Fig. 9(c)] imposed on the reaction products detected at small forward angles do not reveal a pronounced group of events which could be identified unambiguously as the heavy reaction remnants. Even though the fission process is delayed as indicated by the LCP and IMF emission measurements, the cooled nuclei seen late in the deexcitation chain decay predominately by fission.

IV. MODEL CALCULATIONS

In this section, the predictions from two models are discussed and compared with the experimental results. The dynamical aspects of collisions between the projectile and target nuclei (preequilibrium phase) are followed using the computer code CHIMERA [23] which is based upon the molecular dynamics concept. The code is a combination of two recently devised models, namely, the quantum molecular dynamics (QMD) model of Aichelin *et al.* [24] and the quasiparticle dynamics (QPD) model of Boal and Glosli [25]. Recently, the CHIMERA code was applied with the great success to study linear momentum transfer in nuclear reactions for a range of incident energies systems [26]. The comparison of the model calculations with a substantial body of data favors a soft equation of state and the calculations presented in this paper have been performed using the incompressibility of nuclear matter, $K=200$ MeV.

The further history of the excited primary reaction products is simulated by using the Monte Carlo computer code GEMINI [27]. In this code, all possible binary decays of the compound nucleus, from light particle emission to symmetric division, are considered. After each binary splitting, further decay of the resulting excited fragments is continued until all the available excitation energy is exhausted. At each decay step, the remaining excitation energy is divided under the assumption of equal temperatures in the two fragments. Details of these calculations are described in [27].

A. Early phase of the reaction

It has been shown [26] that the time evolution of the longitudinal velocity of the fused system produced in the incomplete fusion reactions approaches its asymptotic value at the end of the preequilibrium phase. This observable was used to establish the time at which one can calculate the characteristics of the equilibrated reaction products (e.g., mass and excitation energy of the composite system produced in the nucleus-nucleus collision).

The time evolution of the ^{63}Cu + ^{232}Th composite system characteristics for the violent collisions ($b<5$ fm) at 35A MeV is shown in Fig. 10. The time $t=0$ fm/c corresponds to the configuration when surfaces of the projectile and target nuclei are separated by 3 fm. Figure 10(a) shows the temporal evolution of the longitudinal momentum carried by the fused system normalized to the linear momentum of the projectile. During the early phase of the collision ($t<120$ fm/c) one can observe a sudden decrease of the longitudinal momentum of the fused system. This behavior is correlated with the high emission rates at the same time interval [Fig. 10(b)]. Figure 10(c) displays the time evolution of the number of nucleons bound in the fused system. In order to estimate at which time instant the preequilibrium emission becomes negligible and the system deexcites statistically, the temporal evolution of the longitudinal velocity of the fused system in the laboratory frame was calculated. An asymptotic value of this quantity is an experimentally investigated observable used to characterize the incompleteness of the fusion process. Figure 10(d) shows that after $t=120$ fm/c the composite system moves with constant velocity which is considerably lower than the value calculated for the com-

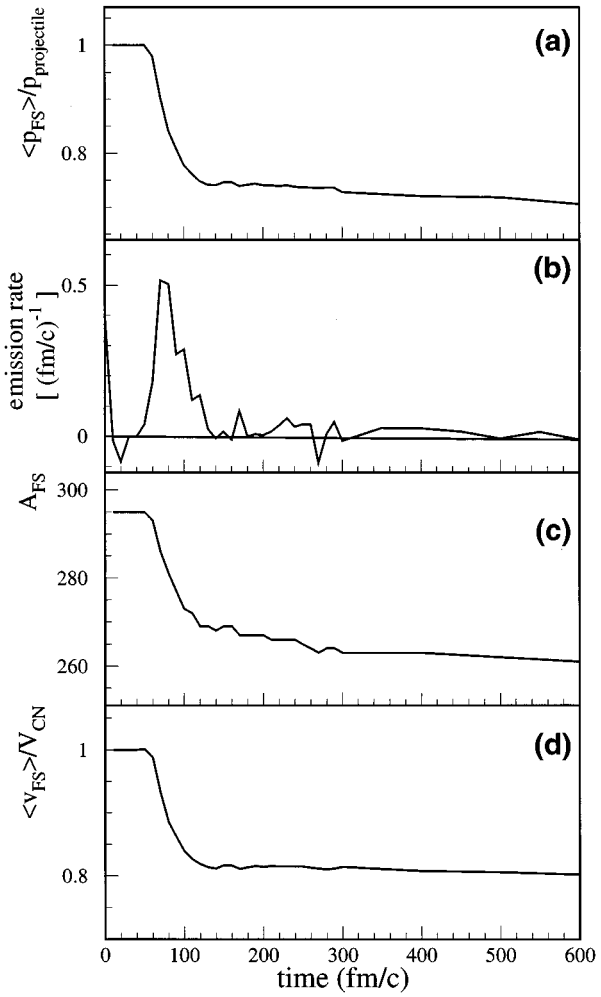

FIG. 10. The CHIMERA code prediction of the time evolution of the ^{63}Cu + ^{232}Th system characteristics for the violent collisions ($b<5$ *fm*) at 35*A* MeV.

plete fusion reaction. The degree of the system equilibration can be quantified by computing the *z*th component of the quadrupole moment tensor of the one-body density in momentum space [18]. The investigation of this quantity shows also that the equilibration of the composite system produced in the violent collision of ^{63}Cu + ^{232}Th at 35*A* MeV is achieved at about 120 fm/*c*. Then, calculating the average value of the mass and velocity of the equilibrated composite system, the LMT for the violent collision was estimated $\approx$73%. This value reproduces well the experimental value of the LMT which was determined in Sec. III A using the folding-angle technique.

The linear momentum transferred to the system is primarily converted into a thermal excitation. In Fig. 2 we present the scatter plot of the number of events versus the percentage of the LMT and the excitation energy calculated by the CHIMERA code at 120 fm/*c*. Here we can see that the model calculations indicate a scenario in which all preequilibrium particles are emitted as separated nucleons for the most violent collisions. On the other hand, in less violent collisions (larger impact parameter) the unfused mass escapes less fragmented.

Figure 11 shows the scatter plots of the number of events for the heaviest fragment mass (upper panel) and for the heaviest fragment excitation energy (lower panel) versus the impact parameter. We note that the highest predicted excitation energy near 950 MeV is attained in the fused system for the most central collisions. The average mass of the composite system was about 273 amu.

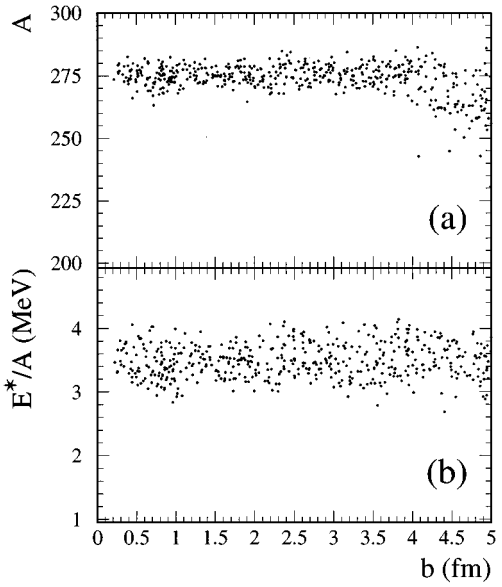

FIG. 11. The scatter plot of the number of events versus the impact parameter and compound nucleus mass [panel (a)] and excitation energy per nucleon [panel (b)] obtained from the CHIMERA code calculations.

The code CHIMERA cannot be used to study the asymptotic properties of the reaction products due to the extremely long computer time required and possible error propagation. Nevertheless, the continuation of the calculations with this code up to one order of magnitude longer in time (3000 fm/*c*) is a tractable task. Such calculations can give an intuitive picture of further reaction scenario in terms of the same model.

Figure 12 presents the probabilities of fission, composite system survival, and fission with IMF emission, calculated at different time instants. Central collisions with the impact parameters below 5 fm were selected. Here, one can observe that over 60% of the composite systems decays before $t=10^{-20}$ s and that about 15% of fission decay is associated with IMF emission. A closer inspection of the reaction simulation reveals that the emission of the IMF takes place both from the composite system before the fission decay and from the neck between two fission fragments at the time of fission.

B. Asymptotic properties of reaction products

The model calculations presented in the former section indicate that the composite system produced in the violent collisions of ^{63}Cu + ^{232}Th at 35*A* MeV equilibrates after about 120 fm/*c*. In order to trace the further evolution of the system, the statistical code GEMINI [27] has been emloyed. Here, the output of the CHIMERA code (i.e., *A*, *Z*, excitation energy and angular momentum of all the fragments) at the time instant 120 fm/*c* has been taken as an input to the GEMINI simulations. The results of the CHIMERA-GEMINI model calculations presented in this section are limited to the central collisions ($b<$ 5 fm).

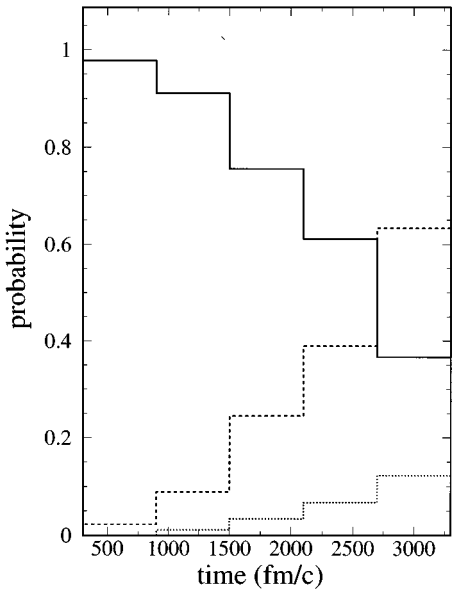

FIG. 12. The calculated probabilities of the fission (dashed line), compound nucleus survivals (solid line), and fission accompanied by the IMF emission (dotted line). The results are obtained with the code CHIMERA.

Figure 13 shows the scatter plots of the mass and velocity of the final cold reaction products. The results in the upper panel were obtained with no dynamic fission delay. Those in the lower panel are for a fission delay time of 10^{-20} s. We note that for both simulations an island of fission events with $60 < A < 120$ and $1.0 < V < 3.0$ cm/ns is present. However, the heavy residue survivals with $130 < A < 180$ and $1.0 < V < 2.0$ cm/ns are produced if the fission delay is introduced. The predicted region of the surviving heavy residue also was indicated in Fig. 9 where the experimental data are presented. While the model indicated that some fission delay

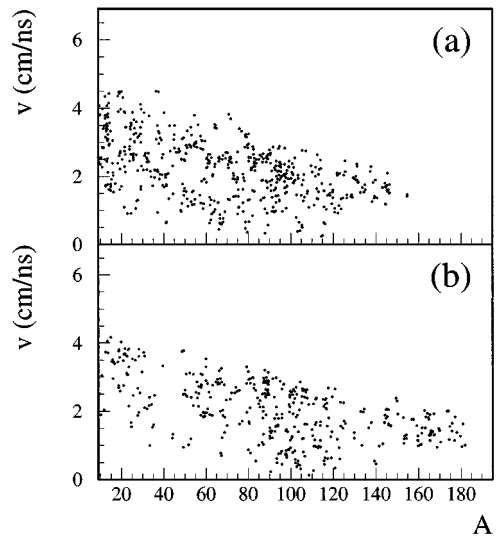

FIG. 13. The scatter plot of the number of events versus the mass and velocity of the heavy fragment obtained from the CHIMERA-GEMINI simulation with no dynamic fission delay (a) and with $\times 10^{-20}$ s dynamic fission delay (b).

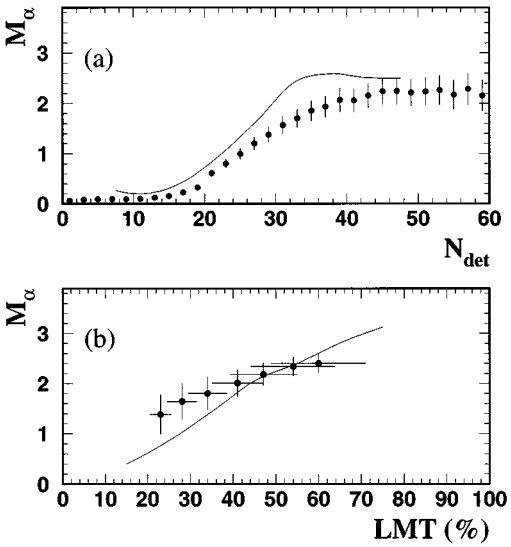

FIG. 14. The α particle multiplicities as a function of the average number of the detected neutrons (a) and on the LMT (b). The experimental data are shown by the dots and the results of the CHIMERA-GEMINI simulations are displayed by the lines.

is required to produce such heavy residues, we have already noted in Sec. III D that, given the low cross section for heavy fragments detected in the high mass region, a convincing verification of the mechanism of their production is difficult. It may be that for nuclei with such compact saddle point shapes the prescission emission does little to modify the fission probability. This dynamical consideration is not well modeled by a fixed delay time in the statistical code. On the other hand, model calculations predict properties of the detected fission products well.

The CHIMERA-GEMINI model calculations of the neutron multiplicities gated on the folding angle and on the IMF's detected in the backward hemisphere are shown in Figs. 7(e) and 7(f), respectively. In this simulation we used the inverse level density parameter $K = 10$ and we applied a fission delay time of 10^{-20} s. This value of the fission delay time was chosen in order to be in agreement with the experimental observation that the heavy residues are produced with much lower probability than the fission fragments. The dotted lines in Figs. 7(e) and 7(f) show the calculated primary distributions of emitted neutrons and the dashed lines were obtained when the detection filter was applied. The results of the CHIMERA-GEMINI model calculations, after being filtered through the experimental conditions, are in satisfactory agreement with the experimental neutron distributions, although for the neutron multiplicity gated on the folding angle, the model calculations slightly underpredict the experimental data. The widths of the experimental neutron distributions are larger than those from the model calculations, which suggests too small an excitation energy dispersion given by the model.

The dependence of the observed α particle multiplicities M_α on the number of the detected neutrons, $N_{\rm det}$, and on the LMT are also reproduced reasonably well by the model calculations [see Figs. 14(a) and 14(b), respectively].

In conclusion, the hybrid CHIMERA-GEMINI code appears to be a good tool to simulate the violent collisions between heavy ions in the intermediate energy domain.

V. DISCUSSION AND CONCLUSIONS

We have studied the properties and decay of hot and heavy composite nuclei produced in the violent collisions between ^{63}Cu and ^{232}Th at 35*A* MeV. The excitation energy that can be deposited into the compound system has been evaluated using fission fragment correlation measurements and coincident detection of the ejectiles and heavy reaction products. From both methods we have concluded that a composite system with an excitation energy close to 1 GeV is formed. This result is in good agreement with dynamical model calculations using code CHIMERA. The mass of the composite system produced in the most violent collisions was estimated as 275 amu.

A dominant decay mode of these hot and heavy nuclei is fission accompanied by a large number of emitted neutrons and charged particles. Approximately one in three of the fission events is associated with the emission of IMF's. A most probable number of 51 ± 3 neutrons is emitted in collisions when the largest value of the linear momentum is transferred and ~9 out of this number are emitted in the preequilibrium phase. The LMT is correlated with the neutron, LCP, and IMF multiplicities and can be used as a indicator of the energy deposited. However, at the higher excitation energies the sensitivity of the neutron multiplicity gauge to the excitation of the nuclei decreases. In order to obtain better quantitative information about the excitation energy the charged particle and fragment emission must also be taken into account.

The initial temperature of the system was estimated from the α particle and IMF energy spectra. The alpha particles are emitted in a long deexcitation chain and in order to convert the slope temperature into the initial temperature we applied the procedure developed in Ref. [28]. Here, we take advantage of the observation that the light particle multiplicities scale linearly with the excitation energy per nucleon of their emitters. Using this procedure, we find that the initial temperature of the α particle emitters produced in the most violent collision is equal to 6.5 ± 0.5 MeV. The temperatures of the IMF emission sources were also evaluated from the IMF spectral slope temperatures in terms of the random walk in momentum space model [16]. The model calculation gives an IMF emission source temperature of 6.0 MeV for $Z_{\mathrm{IMF}}>3$.

The analysis of the events in which a heavy fragment is detected at small forward angles suggests but does not prove that evaporation residues resulting from the decay of the hottest composite systems were observed.

The dynamical aspects of the collisions between the projectile and target nuclei were investigated in terms of a dynamical model CHIMERA and asymptotic characteristics of the reaction product were confronted with the hybrid CHIMERA plus GEMINI codes. The output of the CHIMERA code at the time instant when equilibration was achieved (120 fm/c) has been taken as an input to the GEMINI simulations. A comparison between the model calculations and the experimental data shows that the hybrid CHIMERA-GEMINI code is a good tool to simulate the violent collisions between heavy ions in the intermediate energy domain.

ACKNOWLEDGMENTS

We thank R. J. Charity for providing us with the GEMINI code. We appreciate the efforts of the technical staff of the TAMU Cyclotron Institute for their excellent job during our beam time. The work was supported by the Polish Scientific Research Committee under Grant No. 2 2392 91 02, by the Department of Energy under Grant No. DE-FG05-86ER40256, by the National Science Foundation, and by the Robert A. Welch Foundation.

[1] H. Stöcker and W. Greiner, Phys. Rep. **202**, 233 (1991).
[2] P. Bonche, S. Levit, and D. Vautherin, Nucl. Phys. **A436**, 265 (1985).
[3] Z. Majka *et al.*, in *Proceedings of the ACS Nuclear Chemistry Award Symposium*, Anaheim, California, 1995, edited by G. Nebbia and M. N. Namboodiri (World Scientific, Singapore, 1995), p. 63.
[4] R. P. Schmitt *et al.*, Nucl. Instrum. Methods Phys. Res. A **354**, 487 (1995).
[5] J. Łukasik, Z. Micek, Z. Sosin, A. Wieloch, and K. Grotowski, Nucl. Instrum. Methods Phys. Res. A **274**, 265 (1989).
[6] J. Poitou and C. Signarbieux, Nucl. Instrum. Methods **114**, 113 (1974).
[7] B. J. Hurst (private communication).
[8] D. Utley, R. Wada, K. Hagel, X. Bin, M. Gui, Y. Lou, R. Tezkratt, J. B. Natowitz, and M. Gonin, Phys. Rev. C **49**, R1737 (1994).
[9] D. Jacquet *et al.*, Phys. Rev. Lett. **53**, 2226 (1984); M. Conjeaud, S. Harrar, M. Mostefai, E. C. Pollacco, C. Volant, Y. Cassagnou, R. Dayras, R. Legrain, H. Oeschler, and F. Saint–Laurent, Phys. Lett. **159B**, 244 (1985); D. X. Jiang *et al.*, Nucl. Phys. **A503**, 560 (1989); E. C. Pollacco, C. Volant, Y. Cassagnou, M. Conjeaud, R. Dayras, S. Harrar, R. Legrain, and J. -E. Sauvestre, Z. Phys. A **346**, 62 (1993); E. Schiwnn *et al.*, Nucl. Phys. **A568**, 169 (1994); J. Galin and U. Jahnke, J. Phys. G **20**, 1105 (1994).
[10] E. E. Gualtieri *et al.*, Phys. Lett. B **357**, 7 (1995).
[11] M. Gonin *et al.*, Phys. Lett. B **217**, 406 (1989); M. Gonin *et al.*, Phys. Rev. C **42**, 2125 (1988).
[12] F. Gramegna (private communication).
[13] L. G. Moretto and G. J. Wozniak, Annu. Rev. Nucl. Part. Sci. **43**, 379 (1993).
[14] A. S. Goldhaber, Phys. Rev. C **17**, 2243 (1978).
[15] S. Bjornholm, in Proceedings of the Nuclear Workshop, I.C.T.P., Trieste, Italy, 1981 (unpublished), p. 521.
[16] W. Bauer, Phys. Rev. C **51**, 803 (1995).
[17] Z. Majka (unpublished).
[18] J. Łukasik, Z. Majka, and T. Kozik, Phys. Lett. B **318**, 419 (1993).
[19] E. Duek *et al.*, Z. Phys. A **317**, 83 (1984); L. Schad, H. Ho, G. -Y. Fan, B. Lindl, A. Pfoh, R. Wolski, and J. P. Wurm, *ibid.* **318**, 179 (1984); M. Sowiński, M. Lewitowicz, R. Kupczak, A. Jankowski, N. K. Skobelev, S. Chojnacki, *ibid.* **324**, 87 (1986); B. Lindl, A. Brucker, M. Bantel, H. Ho, R. Muffler, L. Schad, M. G. Trauth, and J. P. Wurm, *ibid.* **328**, 85 (1987); H.

Ikezoe *et al.*, Nucl. Phys. **A538**, 299c (1992); K. Siwek-Wilczyńska, J. Wilczyński, H. K. W. Leegte, R. H. Siemssen, H. W. Wilschut, K. Grotowski, A. Panasiewicz, Z. Sosin, and A. Wieloch, Phys. Rev. C **48**, 228 (1993).

[20] U. Jahnke, G. Ingold, D. Hilscher, M. Lehman, E. Schwinn, and P. Zank, Phys. Rev. Lett. **57**, 190 (1986).

[21] K. Aleklett *et al.*, in *Proceedings of the International Symposium on Heavy Ion Physics and its Applications*, Lanzhou, China, 1990, edited by W.Q. Shen, Y.X. Luo, and J.Y. Liu (World Scientific, Singapore, 1991), p. 140.

[22] E.C. Pollacco *et al.*, Report No. DAPNIA/SPhN 94 02 1994, and references quoted therein.

[23] J. Łukasik and Z. Majka, Acta Phys. Pol. B **24**, 1959 (1993).

[24] J. Aichelin, G. Peilert, A. Bohnet, A. Rosenhauer, H. Stöcker, and W. Greiner, Phys. Rev. C **37**, 2451 (1988) G. Peilert, H. Stöcker, W. Greiner, A. Rosenhauer, A. Bohnet, and J. Aichelin, *ibid.* **39**, 1402 (1989); J. Aichelin, Phys. Rep. **202**, 233 (1991).

[25] D. H. Boal and J. N. Glosli, Phys. Rev. C **38**, 1870 (1988); **38**, 2621 (1988).

[26] J. Cibor, J. Łukasik, and Z. Majka, Z. Phys. A **348**, 233 (1994).

[27] R. J. Charity *et al.*, Nucl. Phys. **A483**, 371 (1988).

[28] R. Wada *et al.*, Phys. Rev. C **39**, 497 (1989).